# Flat and self-trapping photonic bands through coupling of two unidirectional edge modes

Yun-tuan Fang,* Han-Qing He, Jian-xia Hu, Lin-kun Chen, and Zhang Wen
*School of Computer Science and Telecommunication Engineering, Jiangsu University, Zhenjiang 212013, China*
(Received 18 November 2014; published 23 March 2015)

We find a flat band and a self-trapping band through the coupling of two unidirectional edge modes, which was originally achieved by Wang *et al.* [Phys. Rev. Lett. **100**, 013905 (2008); Nature **461**, 772 (2009)] in two-dimensional magneto-optical photonic crystals. We break up a square-lattice yttrium-iron-garnet photonic crystal forming a waveguide and two edges. Given a proper interval of the two edges, two unidirectional edge modes with opposite group velocity directions can be coupled. The coupling leads to a wide flat band in which the group velocity is near zero, and a self-trapping band in which light is totally localized around the source. The position of the flat band and the group velocity can be adjusted by the external magnetic field. Numerical simulations and theoretical analysis both demonstrate the two interesting band structures.

DOI: 10.1103/PhysRevA.91.033827 PACS number(s): 42.70.Qs, 42.25.Gy, 41.20.Jb, 78.20.Ls

## I. INTRODUCTION

In 2008, Raghu and Haldane [1,2] predicted the existence of one-way electromagnetic modes in two-dimensional (2D) magneto-optical (MO) photonic crystals (PCs) similar to the chiral edge states found in the integer quantum Hall (QH) effect. These modes are confined at the edge of certain 2D MO photonic crystals and possess group velocities pointing in only one direction, determined by the direction of an applied dc magnetic field. Backscattering in the unidirectional edge modes is completely suppressed. These modes are very important for slow-light structures, which are susceptible to backscattering. After that, Wang *et al.* demonstrated the existence of the unidirectional edge modes through experimental and theoretical study [3,4]. They further proved that such chiral edge states are robust against scattering from disorder. Because the edge modes are inside the light cone, to avoid light scattering into the air, a nonmagnetic metallic cladding or another photonic crystal has to be bound on one side of the edge of the 2D MO PC. Some similar studies have been proposed [5–8]. In this paper we perform a study on the coupling of the two unidirectional edge modes. As is well known, the coupling among different modes may excite many new and interesting phenomena [9]. Through the study we find that a flat photonic band and even a self-trapping photonic band occur from the coupling.

## II. CALCULATION METHOD AND ISOLATED EDGE MODES

The edge modes and their coupled modes of the 2D MO PC can be obtained from the modified plane wave expansion method. An external dc magnetic field applied in the out-of-plane ($z$) direction induces strong gyromagnetic anisotropy, with the permeability tensor taking the form [3]

$$\mu(\mathbf{r}) = \begin{bmatrix} \mu_1 & j\mu_2 & 0 \\ -j\mu_2 & \mu_1 & 0 \\ 0 & 0 & \mu_3 \end{bmatrix}. \tag{1}$$

For **E** polarization (the electric field is along the $z$ axis), we eliminate the magnetic field from Maxwell's equations to obtain the master equation,

$$\nabla \times \frac{1}{\mu(\mathbf{r})} \nabla \times \mathbf{E}(\mathbf{r}) = \omega^2 \varepsilon_0 \mu_0 \mathbf{E}(\mathbf{r}) = \frac{\omega^2}{c^2} \mathbf{E}(\mathbf{r}), \tag{2}$$

where $\frac{1}{\mu(\mathbf{r})} = \begin{bmatrix} \mu' & j\mu'' & 0 \\ -j\mu'' & \mu' & 0 \\ 0 & 0 & \mu''' \end{bmatrix}$ is the position-dependent periodic structure in the $xy$ plane. Taking advantage of the periodic nature of the problem, the $E$ field may be expanded into a sum of plane waves using Bloch's theorem as

$$E_z(\mathbf{r}) = \sum_{\mathbf{G}} E(\mathbf{k}+\mathbf{G}) \exp[i(\mathbf{k}+\mathbf{G}) \cdot \mathbf{r}], \tag{3}$$

where $\boldsymbol{k}$ is a wave vector in the Brillouin zone; $\boldsymbol{G}$ represents a lattice vector in reciprocal space, describing the periodic structure; and $\boldsymbol{E}(\boldsymbol{k}+G)$ is the expansion coefficient corresponding to $\boldsymbol{G}$. The tensor elements of $\frac{1}{\mu(\mathbf{r})}$ can be expressed as a Fourier series expansion,

$$\mu' = \sum_{\mathbf{G}} \mu'(\mathbf{G}) \exp(i\mathbf{G} \cdot \mathbf{r}), \tag{4}$$

$$\mu'' = \sum_{\mathbf{G}} \mu''(\mathbf{G}) \exp(i\mathbf{G} \cdot \mathbf{r}), \tag{5}$$

where

$$\mu'(\mathbf{G}) = \frac{1}{A_u} \int \mu'(\mathbf{r}) \exp(-i\mathbf{G} \cdot \mathbf{r}) d\mathbf{r}, \tag{6}$$

$$\mu''(\mathbf{G}) = \frac{1}{A_u} \int \mu''(\mathbf{r}) \exp(-i\mathbf{G} \cdot \mathbf{r}) d\mathbf{r}. \tag{7}$$

In (6) and (7) $A_u$ indicates the area of Wigner-Seitz (WS) unit cells that may be used to represent the periodic structure. By taking Eqs. (3)–(5) into (2), we finally obtain

$$\sum_{\mathbf{G}'} [\mu'(\mathbf{G}-\mathbf{G}')\mathbf{K}' \cdot \mathbf{K} - j\mu''(\mathbf{G}-\mathbf{G}')(\mathbf{K}' \times \mathbf{K} \cdot \mathbf{e_z})] E(\mathbf{k}+\mathbf{G}') = \frac{\omega^2}{c^2} E(\mathbf{k}+\mathbf{G}), \tag{8}$$

*fang_yt1965@sina.com

 

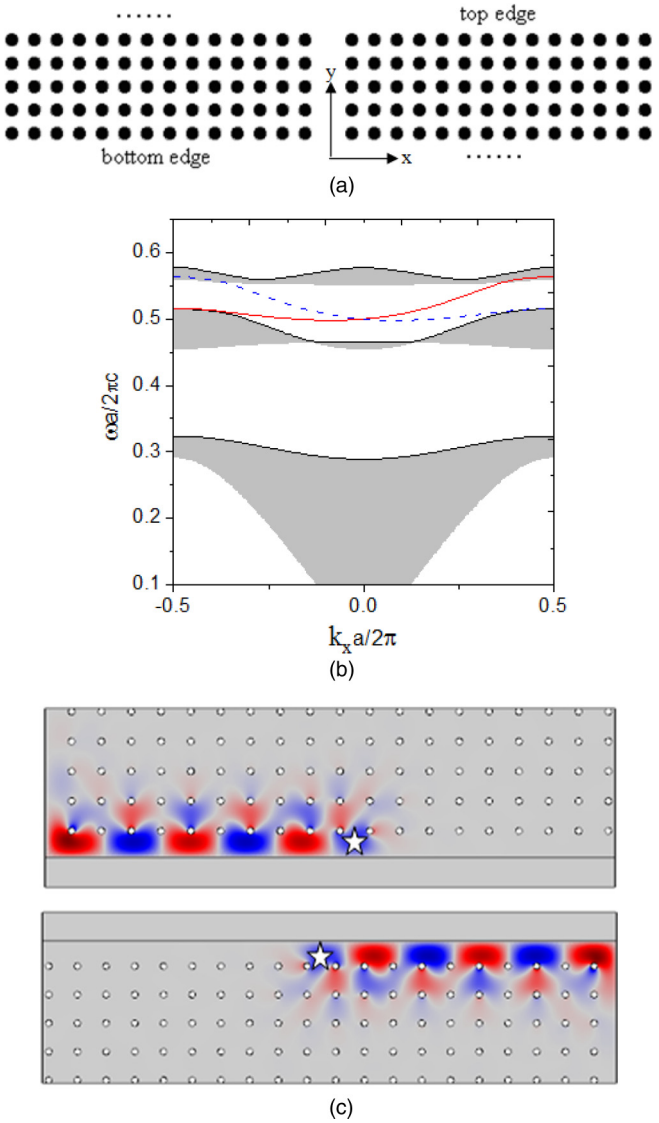


FIG. 1. (Color online) Magneto-optical unidirectional edge modes. (a) 2D MO PC with its two edges in two opposite directions. (b) Projected band diagram for 2D MO PC with metallic cladding. Blue dashed and red solid lines represent the unidirectional edge modes for two different edges, respectively. (c) Steady-state field pattern for each unidirectional edge mode. Red and blue represent positive and negative field values. A source, indicated by a star, is located at the two edges and operates at a frequency $\omega = 0.5426 \times 2\pi c/a$.

where $\mathbf{K} = \mathbf{k} + \mathbf{G}$ and $\mathbf{K}' = \mathbf{k} + \mathbf{G}'$. Equation (8) includes the sum of infinite reciprocal vectors $\mathbf{G}'$ and we select finite reciprocal vectors instead in the allowed precision range. Then the equation becomes a matrix eigenvalue equation. For a fixed wave vector $\boldsymbol{k}$, the frequencies $\omega$ of the allowed modes in the periodic structure are found through solving Eq. (8).

We firstly consider the isolated edge modes. Using gyromagnetic materials, we design a one-way waveguide using a 2D MO square-lattice yttrium-iron-garnet (YIG) PC operating at microwave frequencies. The structure parameters are chosen the same as those in Ref. [3]. The 2D MO PC and its two edges in two directions are shown in Fig. 1(a). To excite the edge modes a metallic cladding must be bound on one side of the 2D MO PC. The projected band for the edge states is shown in Fig. 1(b). We take $k_x$ as the projection of the 2D wave vector and $a$ is the lattice length. The band structure is symmetric with respect to $k_x = 0$ since the structure itself has inversion symmetry. As is shown in Fig. 1(a), the PC has two edges in two opposite directions: the bottom edge of the upper semi-infinite PC and the top edge of the lower semi-infinite PC. Thus the red solid curve and the dashed blue curve inside the gap of infinite PC correspond to the two isolated edge modes, respectively. It is clearly seen from Fig. 1(b) that the slope of the red curve is always positive, while the slope of the blue curve is always negative, which means that the group velocity for each mode points in only one direction. But the group velocity directions for the two modes are opposite. The isolated one-way edge mode can be further illustrated through the simulations of electromagnetic waves based on the finite element method. A point source (labeled by a star) with $\omega a/2\pi c = 0.54$ is placed at the centers of the two edge waveguides. The distributions of electric field in the $z$ direction are shown in Fig. 1(c). The left transmitted field and right transmitted field correspond to the dashed blue curve and the red solid curve, respectively.

## III. COUPLING OF TWO EDGE MODES

In this paper we focus on the coupling of the two edge modes. To achive it we just break up the 2D MO PC and obtain a line defect waveguide and two edge configurations. Under an applied dc magnetic field, the structure may excite unidirectional edge modes on the two edges of two semi-infinite 2D MO PCs, respectively. If the interval between the two edges is adjusted properly, the two edge modes can be coupled, which results in some new modes. The structure model is shown in Fig. 2. In the band calcutions for the waveguide modes or the coupled edge modes, a supercell must be used just as indicated by the dashed rectangle in Fig. 2. The interval between the two edge rod centers is indicated by $d$. Theoretically, the supercell must contain infinite rods. In

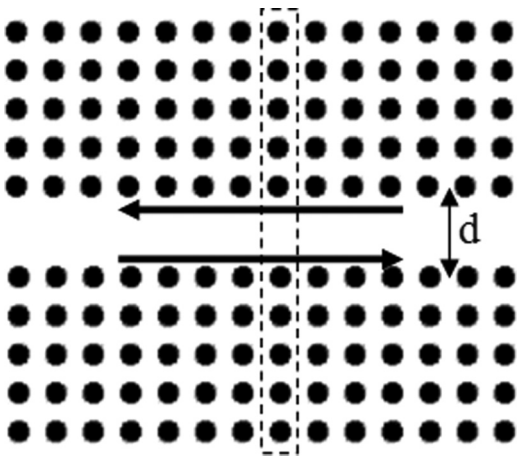


FIG. 2. 2D MO PC with a line defect waveguide. The width of the waveguide is denoted as $d$. Two arrows denote the directions of two isolated unidirectional edge modes. The dashed rectangle denotes a supercell in the calculations.

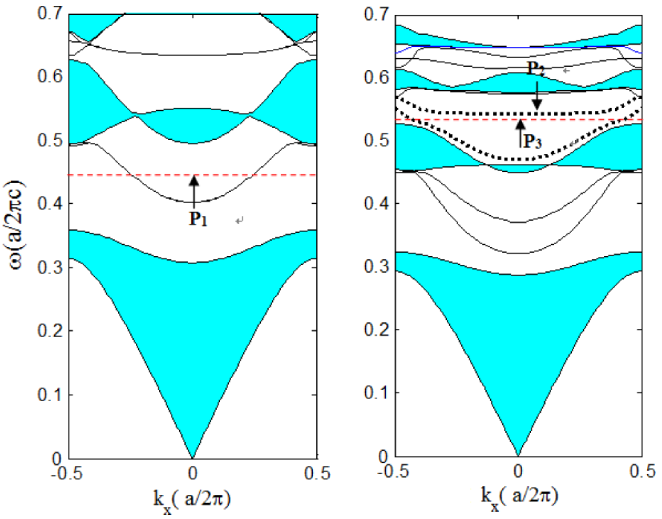


FIG. 3. (Color online) The band diagrams for the structure as Fig. 2 with $d = 1.5a$. There are two cases: without a magnetic field (left plot), and with applied magnetic field in the same directions (right plot) on the two PCs, respectively. $P_1$, $P_2$, and $P_3$ denote three frequencies at different mode dispersion curves.

pratical calculations a finite number of rods can satisfy the needed accuracy.

For the structure in Fig. 2 we consider two cases: without any magnetic field, and with applied magnetic field in the same direcitions on the two PCs, respectively. The band structures with $d = 1.5a$ for the two cases are shown in Fig. 3 in which the blue areas denote the bulk mode bands. The left subplot corresponds to the first case in which two curves inside the band gaps are the waveguide modes. No edge mode occurs in this case. The right subplot corresponds to the second case. From the right subplot case we find two special dashed dispersion curves in the second gap. The two mode curves are the main studied objects in the paper. The upper band is very flat and the flat region occupies most of the 1D Brillouin zone. The lower band is symmetric and has two opposite slop. We first consider the upper band. The flat band means that the group velocities are near zero, thus the light seems to be stopped in the waveguide. The wide superflat band is very important because it can achive near-zero group velocity in the waveguide. Although similar bands have been achieved in Refs. [10–13], the structures in them are very complicated and the designs must be elaborately optimized. The other limitations in them are that the band cannot be modulated and they are sensitive to structure perturbation. The flat band in the current structure results from the coupling of two opposite unidirectional edge modes. Because the chiral edge states are robust against scattering from disorder [1–4], their coupled modes could also be robust against the structure perturbation. The positions of the flat band can be adjusted by changing the value of the nondiagonal element $\mu_2$ which is determined by the external magnetic field. Figure 4 shows the results. As $\mu_2$ decreases, the frequency range of the whole flat band monotonously drops and the band curves tend to have a small slope.

Furthermore, the group velocity for the band can also be modulated by the external magnetic field. For the given

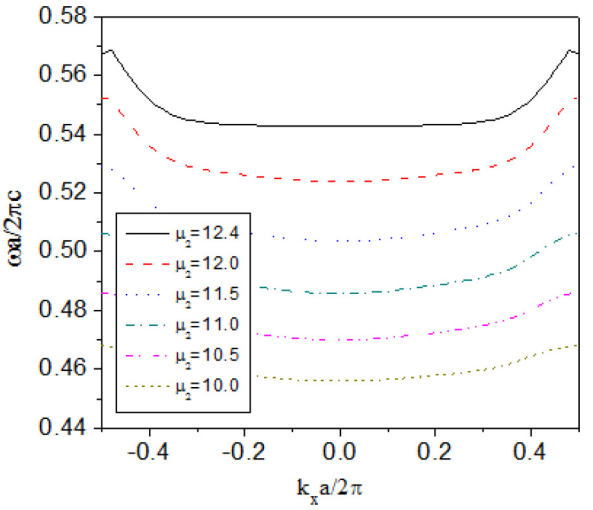


FIG. 4. (Color online) The position change of the upper dashed band in Fig. 3 with the value of the nondiagonal element $\mu_2$.

frequency $\omega = 0.5426(2\pi c/a)$ which is just at the position of the flat part of the band, we calculate the group velocity by calculating $v_g = d\omega/dk_x$ for different values of $\mu_2$. The results are shown in Fig. 5. As $\mu_2$ decreases from 12.4 to 11.95, the group velocity monotonously increases from 0 to $0.20c$. When $\mu_2$ still decreases, the group velocity begins to decrease. The tunability for the flat band and the group velocity makes the system more useful than other similar slow-light waveguides.

For the lower band in the same gap as the flat band, the dispersion curve is symmetric and has large slopes; thus one frequency corresponds to two modes with opposite group velocity directions. The two modes will form a degenerate state. When a source with one frequency is located in the waveguide, two modes with opposite group velocity may be simultaneously excited and interfered. In the following we will study its unique property based on the electromagnetic field simulations.

These field patterns from the electromagnetic field simulations can further reveal the properties of these bands and their

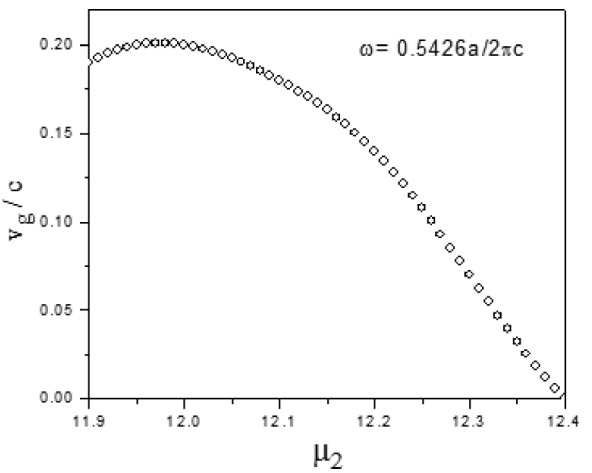


FIG. 5. The group velocity versus $\mu_2$ for $\omega = 0.5426(2\pi c/a)$ which is at the position of the flat band in Fig. 3.

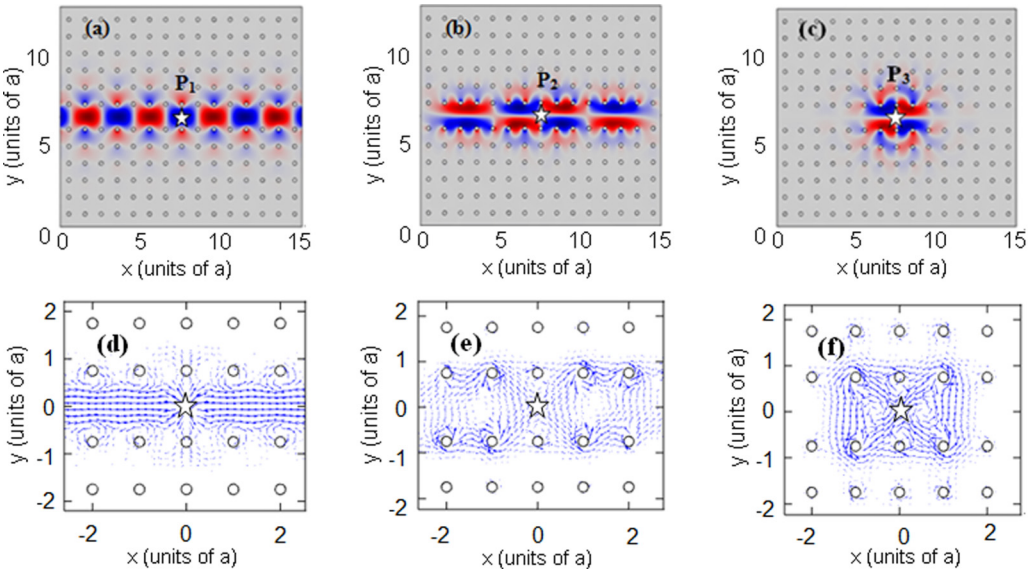


FIG. 6. (Color online) (a–c) The steady-state $\mathbf{E}_z$ field patterns correspond to three mode frequencies $P_1$, $P_2$, and $P_3$ at different mode dispersion curves in Fig. 3. $P_1$ corresponds to a typical waveguide mode. $P_2$ is at the flat band. Its field is along two edges which result from the coupling of two unidirectional edge modes. $P_3$ is at the lower dashed band in Fig. 3. Its field is self-trapped around the source because of the destructive interference of two degenerated modes with opposite group velocity directions. (d–f) The distributions of the Poynting vectors correspond to $P_1$, $P_2$, and $P_3$, respectively.

difference. We choose three frequencies, $P_1(0.45 \times 2\pi c/a)$, $P_2\,(0.5427 \times 2\pi c/a)$, and $P_3(0.5405 \times 2\pi c/a)$, which are on different bands in Fig. 3 (the horizontal dashed lines denote the frequency positions). The steady-state $\mathbf{E}_z$ field patterns for them are plotted in Figs. 6(a)–6(c), respectively. A source, indicated by a star, is located at the center of the waveguide. Blue and red represent positive and negative field values. $P_1$ corresponds to the waveguide mode because there are no any edge modes in the structure. There are two modes with the same frequency; thus it is a generated state. As can be seen, the field is concentrated inside the waveguide and decays quickly from the edges to bulk crystals. Figure 6(d) shows the distribution of the Poynting vectors for $P_1$ near the waveguide. We find the energy flow is concentrated inside the waveguide and point to two opposite directions from the source. $P_2$ and $P_3$ correspond to the coupled modes of two unidirectional edge modes. $P_2$ is just on the flat band. The field pattern for $P_2$ is clearly different from that for $P_1$. As can be seen, the field is mainly concentrated on both edges. We think the waveguide modes are totally suppressed in this gap. $P_2$ corresponds to a single even mode. We can see the field pattern is antisymmetric and it satisfies $\mathbf{E}_z(-\mathbf{r}) = \mathbf{E}_z(\mathbf{r})$ [14]. One may ask what led to the superflat band. We think under current configuration, the source excites two opposite edge modes along each side. Because of the symmetry of two mode dispersion curves, the two modes with the same frequency have the same properties, only with the opposite wave-vector directions. Under a proper interval between the two edges, the two edge modes are coupled to each other. The coupling can lead to a constructive interference and a field similar to a standing wave may be formed on each edge. In Fig. 6 there are clear standing-wave patterns along two edges which means that the flat band comes from the constructive interference of two edge modes. Because the standing waves do not transmit the energy, the band has near-zero group velocity and becomes very flat. The energy flow for $P_2$ shown in Fig. 6(e) is concentrated around the edge rods and forms an anticlockwise loop. The average component of the Poynting vectors in the waveguide direction is near zero.

As for the frequency $P_3$ that is on the lower coupled band, an interesting feature is found from Fig. 6 that not only in the vertical direction but also in the horizontal waveguide direction the field is localized. There seems to be a cavity around the source. However, there is no barrier in the waveguide direction. Thus light seems to be self-trapped in the waveguide. The ability to confine light is important both scientifically and technologically. Although many light confinement methods exist, they all achieve confinement with materials or systems such as metallic mirrors, photonic band-gap materials, and highly disordered media (Anderson localization). In 2013 Hsu *et al.* achieved light confinement in a patterned dielectric slab, even though outgoing waves are allowed in the surrounding medium. Such bound states are called "embedded eigenvalues" which are in a continuum of radiation modes [15,16]. Authors attributed the bound state to the destructive interference of the forward- and back-reflected leakage waves which cancel the radiation amplitudes. However, the embedded eigenvalues only occur at some special $k$ points over the first Brillouin zone. The ideas in Refs. [15,16] help us analyze our results. In the current structure, light is confined in the vertical direction because of the effect of the photonic band gap, but light radiation is usually allowed in the waveguide direction. Thus the localized state for $P_3$ can be looked at as another kind of embedded eigenvalue. As is known, for $P_3$ two coupled modes with the opposite group velocity directions may be simultaneously excited and interfere with each other. Just as the "embedded eigenvalues" which are due to the destructive interference of the forward- and back-reflected leakage waves, the light self-trapping in the waveguide direction is also

because of the destructive interference of the forward- and back-reflected coupled waves. The destructive interference cancels the radiation amplitude along the waveguide. By checking the Poynting vector distribution, we find the Poynting vectors only occur around the source and the neighbor six rods. More interesting, the Poynting vectors make the large anticlockwise loop around the periphery of the six rods and the small anticlockwise loop around each rod. We also find that the light self-trapping state is not only at $P_3$. For frequencies within the lower dashed band of the middle subplot of Fig. 3 and the gap, as well as below the flat band, all point sources will excite the self-trapping state. Thus we call the lower dashed band as a self-trapping band.

We can give an analytical description of the system to gain a physical understanding of the flat and self-trapping bands. A convenient and effective approach is the coupled oscillator model which describes a coupling behavior of the two original isolated edge modes in the system. The detailed description for the model can refer to Refs. [17,18]. The system can be represented as two degenerated edge modes. The Hamiltonian of the coupled system can be written as follows:

$$H = \begin{bmatrix} \omega_k & \Omega \\ \Omega & \omega_{-k} \end{bmatrix}, \tag{9}$$

where $\omega_k$ and $\omega_{-k}$ are the eigenfrequencies of the uncoupled edge modes which have the opposite wave vectors, and $\Omega$ denotes the coupling strength of the two edge modes. Eq. (9) lead to an eigenmatrix equation. The eigenvalues $\omega$ of the Hamiltonian represent the new eigenfrequencies of the coupled system which can be obtained from the equation

$$\begin{vmatrix} \omega - \omega_k & \Omega \\ \Omega & \omega - \omega_{-k} \end{vmatrix} = 0. \tag{10}$$

Because of $\omega_k = \omega_{-k}$, we have $\omega = \omega_k \pm \Omega$ and obtain two branch coupled mode bands. Because the coupling strength is dependent on the difference of the two edge modes, i.e., the value of $k_x$, the less the value of $k_x$, the more the value of $\Omega$. From Fig. 1 we see that $\omega_k$ monotonously decreases as $k_x$ decreases. Thus the branch formed by $\omega = \omega_k + \Omega$ remains flat, whereas the other branch formed by $\omega = \omega_k - \Omega$ drops quickly as $k_x$ decreases. Therefore, the flat and self-trapping bands are in agreement with the coupled oscillator model analysis.

## IV. CONCLUSIONS

In this paper we construct a configuration of a 2D MO PC to achieve the coupling of two unidirectional edge modes. Given proper structure parameters, we can obtain a tunable superflat band and a self-trapping band. The photonic modes in the two bands are clearly different from general waveguide modes. The near-zero group velocity and self-trapping function for the two interesting bands may find their important applications in functional devices such as switches, optical delay lines, and all-optical storage.

## ACKNOWLEDGMENTS

This work was supported by the Senior Talent Foundation of Jiangsu University under Grant No. 13JDG003.

[1] S. Raghu and F. D. M. Haldane, Phys. Rev. A **78**, 033834 (2008).
[2] F. D. M. Haldane and S. Raghu, Phys. Rev. Lett. **100**, 013904 (2008).
[3] Z. Wang, Y. D. Chong, J. D. Joannopoulos, and M. Soljacic, Phys. Rev. Lett. **100**, 013905 (2008).
[4] Z. Wang, Y. D. Chong, J. D. Joannopoulos, and M. Soljacic, Nature **461**, 772 (2009).
[5] K. Fang, Z. Yu, and S. Fan, Nat. Photonics **6**, 782 (2012).
[6] M. Hafezi, E. A. Demler, M. D. Lukin, and J. M. Taylor, Nat. Phys. **7**, 907 (2011).
[7] A. B. Khanikaev, S. H. Mousavi, W. K. Tse, M. Kargarian, A. H. Macdonald, and G. Shvets, Nat. Mater. **12**, 233 (2013).
[8] M. C. Rechtsman, J. M. Zeuner, Y. Plotnik, Y. Lumer, D. Podolsky, F. Dreisow, S. Nolte, M. Segev, and A. Szameit, Nature **496**, 196 (2013).
[9] R. O. Umucalılar and I. Carusotto, Phys. Rev. A **84**, 043804 (2011).
[10] J. Li, T. P. White, L. O'Faolain, A. Gomez-Iglesias, and T. F. Krauss, Opt. Express **16**, 6227 (2008).
[11] L. H. Frandsen, A. V. Lavrinenko, J. Fage-Pedersen, and P. I. Borel, Opt. Express **14**, 9444 (2006).
[12] A. Y. Petrov and M. Eich, Appl. Phys. Lett. **85**, 4866 (2004).
[13] D. Jukić, H. Buljan, D. H. Lee, J. D. Joannopoulos, and M. Soljačić, Opt. Lett. **37**, 5262 (2012).
[14] J. D. Joannopoulos, R. D. Meade, and J. N. Winn, *Photonic Crystals: Molding the Flow of Light* (Princeton University Press, Princeton, NJ, 1995).
[15] C. W. Hsu, B. Zhen, J. Lee, S.-L. Chua, S. G. Johnson, J. D. Joannopoulos, and M. Soljačić, Nature **499**, 188 (2013).
[16] C. W. Hsu, B. Zhen, S.-L. Chua, S. G. Johnson, J. D. Joannopoulos, and M. Soljačić, Light: Sci. Appl. **2**, e84 (2013).
[17] M. Kaliteevski, S. Brand, R. A. Abram, I. Iorsh, A. V. Kavokin, and I. A. Shelykh, Appl. Phys. Lett. **95**, 251108 (2009).
[18] A. Christ, S. G. Tikhodeev, N. A. Gippius, J. Kuhl, and H. Giessen, Phys. Rev. Lett. **91**, 183901 (2003).